Low-dose phase contrast mammography with conventional x-ray sources

A. Olivo[1*], S. Gkoumas[1], M. Endrizzi[1], C. K. Hagen[1], M. B. Szafraniec[1], P. C. Diemoz[1], P. R. T. Munro[2,3], K. Ignatyev[4], B. Johnson[5], J. A. Horrocks[5], S. J. Vinnicombe[6], J. L. Jones[7], R. D. Speller[1]

[1]Department of Medical Physics and Bioengineering, UCL, Gower St, London WC1E 6BT, UK

[2]Optical and Biomedical Engineering Laboratory, School of Electrical, Electronic and Computer Engineering, The University of Western Australia, 35 Stirling Highway, Crawley, Western Australia 6009, Australia

[3]Centre for Microscopy, Characterization and Analysis, The University of Western Australia, 35 Stirling Highway, Crawley, Western Australia 6009, Australia

[4]Diamond Light Source, OX11 0DE, Didcot, UK

[5]Clinical Physics, St Bartholomew's Hospital, Barts Health NHS Trust, London EC1A 7BE, UK

[6]Division of Cancer Research, Medical Research Institute, University of Dundee, Dundee DD1 9SY, UK

[7]Centre for Tumour Biology, Queen Mary, University of London, John Vane Science Centre, London EC1M 6BQ, UK

[*]corresponding author: email a.olivo@ucl.ac.uk, tel +44 (0)20 7679 2444, fax +44 (0)20 7679 0255

Abstract

Purpose: to provide an X-ray Phase Contrast Imaging (XPCI) method working with conventional sources that could be readily translated into clinical practice. XPCI shows potential in synchrotron studies but attempts at translating it for use with conventional sources are subject to limitations in terms of field of view, stability, exposure time and, possibly most importantly, delivered dose.

Methods: following the adaptation of our "edge-illumination" XPCI technique for use with conventional x-ray sources through the use of x-ray masks, we have further modified the design of such masks to allow further reducing the dose delivered to the sample without affecting the phase sensitivity of the method.

Results: we have built a prototype based on the new mask design and used it to image *ex-vivo* breast tissue samples containing malignant lesions. We compared images acquired with this prototype to those obtained with a conventional system. We demonstrate and quantify image improvements, especially in terms of microcalcification detection. On calcifications detected also by the conventional system, we measure contrast increases from 5 to 9 fold; calcifications and other features were also detected which are completely invisible in the conventional image. Dose measurements confirmed that the above enhancements were achieved while delivering doses compatible with clinical practice.

Conclusions: we obtained phase-related image enhancements in mammography by means of a system built with components available off-the-shelf that operates under exposure time and dose conditions compatible with clinical practice. This opens the way to a straightforward translation of phase enhanced imaging methods into clinical practice.

Keywords: mammography, x-ray phase contrast imaging, microcalcifications, image contrast

Introduction

X-ray phase contrast imaging (XPCi) generates contrast from refraction and interference[1-3], overcoming the problem of low image contrast resulting from small attenuation differences. This was shown to be beneficial in medical imaging,[3,4] mammography[4,5] in particular. For years, XPCi was considered restricted to synchrotrons, where XPCi mammography has reached the *in vivo* stage.[5] The diagnostic improvements demonstrated by this *in vivo* study prove the importance of implementing XPCi mammography outside synchrotrons.

While recent methods enable XPCi with conventional sources, application of these to mammography suffered from excessive exposure time and, crucially, radiation doses too high for clinical practice.

Free-space propagation[2,5,6] requires high spatial coherence (i.e., a source with a small angular diameter as seen from the sample), i.e. either synchrotrons [2,5] or microfocal sources,[6] the latter leading to excessively long exposure times[6] due to low emitted flux. If the focal spot is increased to make more flux available, phase enhancements vanish:[7,8] a clinical translation attempt did "not lead to a statistically significant difference in recall and cancer detection rates", [9] while the Trieste study, which uses the same method but a source of suitable coherence, is demonstrating significant advantages.[5]

Other implementations use crystals[1,10] acting as angular and spectral filters. Although translation attempts exist,[11] crystals select a narrow bandwidth from the conventional source's polychromatic spectrum, again leading to low flux and thus long exposure times.

Grating interferometry,[12,13] based on Talbot self-imaging,[14] still requires high spatial coherence, and is thus subject to the same limitations. However, an extended source can be used by covering it with an additional grating[15] creating an array of individually coherent "sourcelets". Stampanoni *et al.*[16] used this approach to image *ex vivo* breast tissue, and successfully demonstrated improved image quality; however, this required a mean glandular

dose (MGD) one order of magnitude above clinical acceptability. A key reason for this high dose is the absorption analyzer grating placed downstream of the sample. Furthermore, it should be noted that both phase and absorption gratings are manufactured on silicon substrates, which typically are a few hundred micron thick: at least in some configurations, these can thus further increase dose and exposure time. Other restrictions are the flux limitations caused by the "source" grating (necessary if a conventional source is used) and the fine pitch (2-3 μm) of the other gratings, leading to demanding alignment requirements (20-30 nm[17]).

We propose a solution through a modification of the edge-illumination[7] based coded-aperture (CA) approach,[18] the dose-reduction potential of which is due to the pre-sample mask protecting the sample. In this work, we optimize this by combining an open fraction smaller than 50% in the pre-sample mask with small misalignments between pre-sample and detector masks. CA XPCi also offers stability against environmental vibrations, due to larger aperture pitch/dimensions than grating interferometry. This leads to simpler alignment, automated via a feedback mechanism.[19] The source is exploited efficiently as no source grating is required, leading to reduced exposure times,[20] and masks are realized on low-absorbing graphite substrates.

Materials and methods

Figure 1 shows how the CA XPCi concept was modified to achieve low-dose imaging. For simplicity's sake, the parallel-beam geometry is represented, as a divergent beam simply entails scaling down the pre-sample mask. In the "standard" CA XPCi implementation, masks' open fraction is 50%, and a misalignment of half aperture size is used[18,20] (figure 1(a)). Increasing this misalignment enhances sensitivity;[21] however, in this "standard"

configuration, this increases both exposure time and dose, as more primary photons impinge on the absorbing septa of the detector mask.

In the "low dose" version (figure 1(b)), the open fraction of the pre-sample mask is reduced (in this study, to 20%). This enables achieving the same sensitivity, determined by the fraction of the pixel illuminated by the beam[21] (see dashed lines labelled "pixel illumination" in figures 1(a) and 1(b)), with a smaller misalignment between sample and detector masks. A negligible fraction of the beam not stopped by the pre-sample mask thus impinges on the absorbing septa of the detector mask (figure 1(b)). This is the only source of "extra-dose" in CA XPCi, and this configuration enables its minimization. A slight increase in the average beam energy, viable because phase effects decrease more slowly than absorption with increasing energy,[1-3] is used to compensate for this.

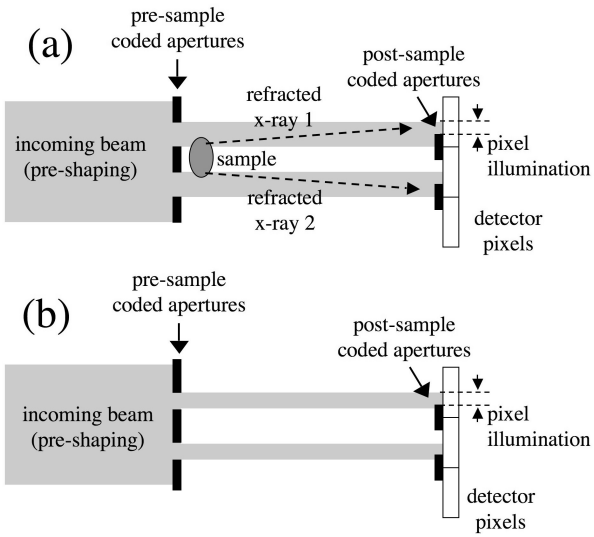

Figure 1 "Standard" (a) vs. low-dose (b) CA XPCi. In the low-dose version, the aperture size in the pre-sample mask is reduced, and a much smaller misalignment between pre-sample and detector mask is adopted. This enables same phase sensitivity to be achieved (determined by the "pixel illumination" indicated by dashed lines in both drawings) while illuminating a very small region of the septa in the detector mask, which is the only source of "additional" dose in CA XPCi.

We also use figure (1) to briefly schematize the method's basic working principle for readers not familiar with it. In Fig 1(a), a sample and two different refracted x-rays (labelled as 1 and 2) have been added. Refraction by the sample causes x-ray 1, which would normally hit the absorbing septa on the detector mask, to be deviated onto the detector pixel and be counted, thus increasing the number of counts in that pixel. The opposite occurs for x-ray 2, which normally would be counted, but is refracted by the sample onto the absorbing septa (thus reducing the number of counts in the corresponding pixel). A similar situation is encountered in the configuration show in figure 1(b), with a prevalence of "x-ray 2" type cases (intensity reduction) due to the introduced asymmetry. This last aspect is specific of the new "low dose" implementation of the method presented in this paper, and is thus further discussed below (see Fig. 4 and related discussion, and supplementary material).

We used the Rigaku M007 source, with molybdenum target and 70 μm focal spot, at 40 kVp and 25 mA, with additional 30 μm molybdenum filtration. The detector is the ANRAD "SMAM" amorphous selenium flat panel, with 85 μm pixel. The pre-sample mask consisted of a series of 720 4.8 cm long, 12 μm wide apertures, with 66.8 μm pitch, obtained in a 30 μm thick gold layer electroplated on a graphite substrate. The detector mask had the same gold thickness and a similar design, but with 6 cm long, 20 μm wide apertures and 83.5 μm pitch. Both masks were manufactured to the authors' design by Creatv Microtech (Lake Potomac, MD). Mask alignment was achieved via a stack of Newport translation stages and Kohzu cradles.[19] The source-to-sample and sample-to-detector distances were 1.6 m and 0.4 m, respectively.

Entrance dose measurements were obtained through a calibrated Keithley 35050A ion chamber positioned immediately downstream of the pre-sample mask, where the sample is normally placed. A 4 cm thick polymethacrylate (PMMA) slab was placed behind the ion

chamber to include contributions from backscattering. The measurements were repeated by means of thermoluminescent dosimeters (TLD-100H), and the same results were obtained to within ~10% accuracy. The additional exposure requested to obtain the same detected statistics on a thicker sample was calculated by assuming a 50%-50% glandular-adipose breast tissue composition; the mass attenuation coefficients for the single elements (H, C, N, O, P) were obtained from the XOP "DABAX" database.[22] Air kerma values were converted into MGD values by using Boone's tabulated factors.[23] The conventional mammographic image was acquired with a GE Senographe Essential Version ADS 54.11, operated at 26 kVp and 25 mAs. Tissue samples were obtained from mastectomies after informed consent; the study was approved by the local ethical regulatory bodies.

Results

Figure 2 shows an example image of a breast tissue specimen obtained with the proposed method (figures 2(b) and 2(c)), compared to conventional mammography (figure 2(a)).

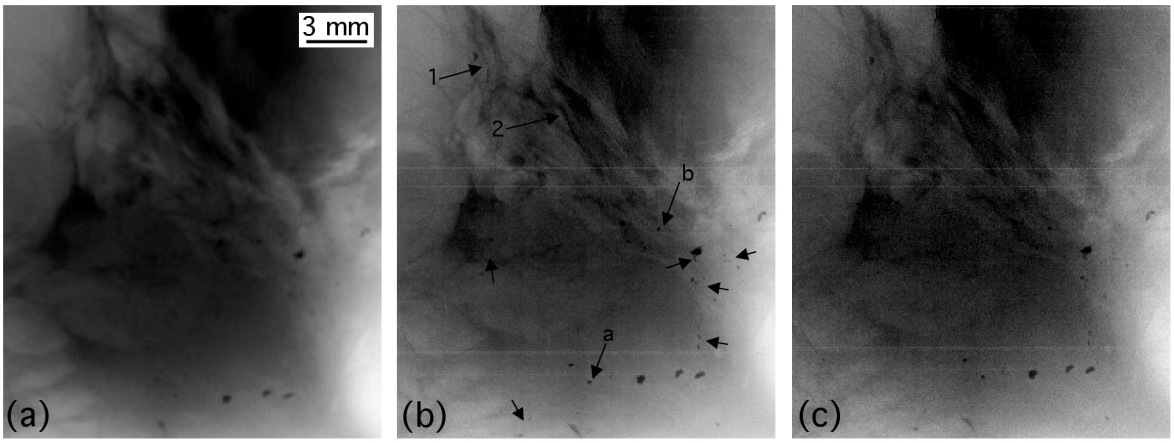

Figure 2. Conventional (a) vs low-dose (b) and ultra-low dose (c) CA XPCi images of the same breast tissue specimen (region of interest extracted from a larger 5 x 5 cm^2 image). Arrows in (b) highlight details of interest: arrows labelled 1 and 2 indicate examples where XPCi leads to improved visualization of the tissue structure (trabeculae in particular); arrows

labelled a and b indicate the calcifications used in the quantitative analysis reported below; unlabelled arrows indicate calcifications or clusters of calcifications invisible in the conventional image. Images should be viewed on a monitor.

Images in figures 2(a), 2(b) and 2(c) were acquired with entrance air kerma values of 3, 5.5 and 1 mGy, respectively, all below the acceptable limit for the entrance dose in mammography (12 mGy[24]). Although this is partly due to the specimen being thinner (~2 cm) than a full breast, extrapolation to thicker samples still leads to clinically acceptable MGD values (see below). By comparing figures 2(a) and 2(b), the increased detail visibility in the XPCi image is apparent, in terms of both tissue definition (arrows labelled "1" and "2") and increased microcalcification detection (unlabelled arrows). Moreover, practically all calcifications detected in Figure 2(b) are still visible in Figure 2(c), obtained at a fifth of the dose. As the pixel size was 100 μm and 85 μm in the conventional and XPCi systems respectively, the increased microcalcification detection is not due to a difference in spatial resolution, but is rather a phase effect: the calcium/soft tissue interface generates x-ray refraction that deviates x-rays on the absorbing septa of the detector mask, thus leading to reduced detected intensity.

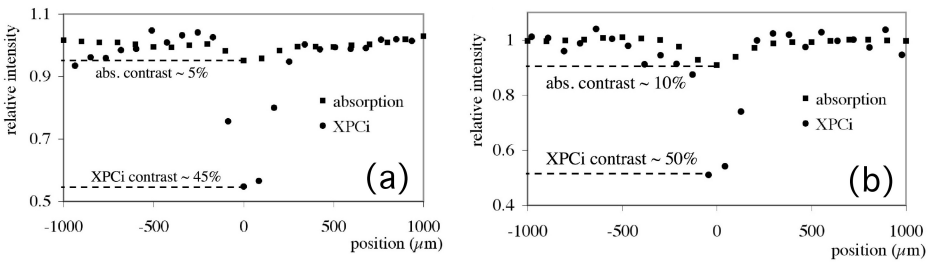

Figure 3. Profiles extracted from figure 2 (a) (squares) and 2 (b) (circles) for the calcifications labelled with "a" and "b" in figure 2 (b). Plots (a) and (b) correspond to calcifications labelled with the same letter in Figure 2 (b). The relative intensity (i.e.

normalized to the background in the immediate vicinity of the calcification) is plotted as a function of the spatial displacement in μm. This enables reading the detail contrast directly on the vertical axis, as the maximum deviation from unity encountered in each plot.

To quantify this, figure 3 shows profiles extracted from two calcifications which are visible both in the conventional and XPCi image (arrows "a" and "b" in figure 2(b)). It should be noted that, for such a direct comparison to be possible, "thicker" calcifications, already presenting an absorption signal sufficient to make them visible also in the conventional image, must be chosen, while the contrast increase is much greater for thinner ones, to the extent that many calcifications are detected which are invisible in Figure 2(a). Also considering this caveat, in the selected examples the contrast increase ranges from 500% (from 10% to 50%, figure 3(b)) to 900% (from 5% to 45%, figure 3(a)). In both graphs, the intensity is plotted against the displacement in μm rather than pixel number, which makes it possible to represent both graphs in the same figure, as the pixel size was slightly different in the two systems (85 vs 100 μm). This exercise of plotting the signals extracted from the calcifications on the same scale, plus the fact that in both cases calcifications are significantly larger than one pixel, further demonstrates that the observed increase in contrast in not related to the (negligible) difference in pixel size between the two systems.

Unlike other "differential" XPCi methods[10,11-13,15] and "standard" CA XPCi[18-21] itself, the profiles in Figure 3 only show a negative peak, rather than a positive/negative pair. This is because the positive peak is generated by the x-rays impinging on the solid septa on the detector mask (figure 1(a)): when sample-induced refraction deviates them into the aperture, they increase the number of detector counts generating a positive peak. These x-rays have been practically eliminated in the low-dose implementation proposed here (figure 2(b)): hence, the only mechanism to generate phase signal is the deviation of x-rays from the

apertures onto the solid septa, which decreases the number of counts creating negative peaks. This is demonstrated in Figure 4, where standard (figure 4(a)) and low-dose (figure 4(b)) CA XPCi images are compared with the conventional absorption image (figure 4(c)) of the same specimen. Profiles were extracted from the same fibrous structure (arrow in figure 4(a)) in all images, and are compared in figure 4(d). While conventional CA XPCi presents the expected double-peak shape (dashed line), the low-dose version (solid line) only features the negative peak. This practically matches the one from the standard CA XPCi image, which is expected as the part of the beam responsible for its formation (the portion falling inside the detector mask apertures) is the same. The fact that this peak is much stronger than the absorption signal extracted from Figure 4(c) (dotted line) demonstrates 1) the almost pure phase nature of the negative peak, and 2) the advantage that the proposed method has also in the visualization of fibrous structures, as well as calcifications. More details on the single vs. double peak formation mechanism are given in the supplementary material.

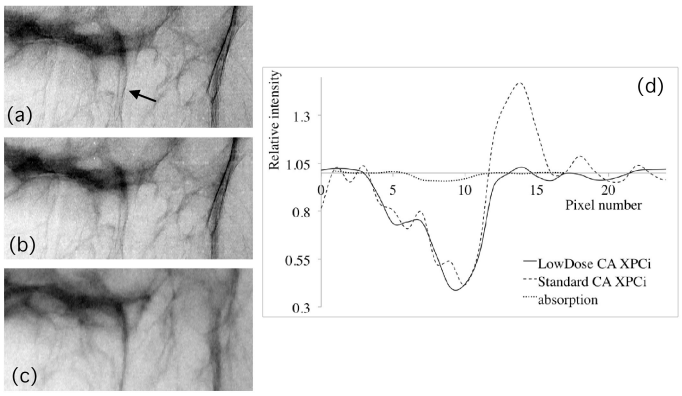

Figure 4 Nature of the signal in low-dose CA XPCi. Panels (a), (b) and (c) show the same tissue specimen imaged with "standard" CA XPCi, low-dose CA XPCi, and conventional absorption imaging, respectively. (d) shows profiles extracted from the same fibrous structure highlighted by the arrow in (a). The negative phase peak practically coincides for standard (dashed line) and low-dose (solid line) CA XPCi, and is much stronger than the absorption

signal extracted from (c) (dotted line). However, the standard CA XPCi profile also shows the positive phase peak, absent from its low-dose correspondent.

If contrast is estimated as peak-to-peak difference, then "standard" CA XPCi doubles it compared to the low-dose implementation, at the price of some additional dose. This can be seen as additional flexibility offered by CA XPCi and, most importantly, the negative peak alone is sufficient to significantly outperform image contrast provided by conventional absorption imaging.

Discussion

To the best of our knowledge, this is the first time non-synchrotron phase-induced enhancements in mammography are obtained at clinically acceptable doses, the closest example being the quoted work of Stampanoni *et al.*[16] which required significantly higher doses.

Horizontal lines visible in figures 2(b) and 2(c) are due to mask defects (actually the current masks have an even larger number of defects, and more than one image was acquired to fill in portions of the sample which were invisible due to this). This could be easily eliminated in a commercial system. Low aspect-ratio masks of this type can be fabricated in sizes compatible with clinical mammography, and are cheap if mass-produced. Another sub-optimal aspect of the current prototype is a maximum detector exposure time of 7 *s*. The image of figure 2(b) was obtained by summing ten 7 *s* frames; that of figure 2(c) by summing two. Each frame contains a comparable number of "dark" counts (counted also with the beam off) and real x-ray hits, leading to penalizing noise propagation when background subtraction is performed. By increasing the number of frames from 2 to 10, we do not obtain the improvement in image quality corresponding to a 5-fold increase in the statistics, and one can estimate that a "real"

10 *s* acquisition would provide the same image quality as summing two 7*s* frames (and would reduce the dose). We are currently operating at 2 m source-to-detector distance, while there is evidence that a 1.5 m long system could provide comparable performance[21] leading to a two-fold reduction in exposure time. Finally, no source optimization was implemented.

For the imaged specimens, we provided entrance air kerma values rather than MGDs due to their limited thickness (~2 cm). At the moment we do not have access to thicker samples. However, an estimation of the MGD that would be required to image e.g. a 4 cm thick specimen (for which the concept of MGD is significant) can be provided in the following way. For the spectrum used (Mo at 40 kVp with 30 μm additional Mo filtration), we have calculated the increase in exposure that would be required to achieve the same statistics on the detector (and therefore, to first approximation, the same image noise) as in the images of Figure 2(b) and 2(c). This was done by assuming a 50%-50% glandular-adipose breast tissue composition for the additional 2 cm of breast, and by obtaining the mass attenuation coefficients for the single elements (H, C, N, O, P) from the XOP "DABAX" database.[22] The increased air kerma values calculated in this way were then converted into MGD values by using Boone's tabulated factors.[23] This lead to MGDs of ~3 and 0.7 mGy (for the statistics of Figure 2(b) and 2(c) respectively), which "bracket" MGD values used in clinical practice, and are both within the limits of quality assurance protocols in mammography.[24] Admittedly this refers to the specific spectral parameters used in this proof-of-concept study (e.g. the kVp setting is higher than normally used in mammography, a choice partly made possible by the fact that phase effects decrease more slowly than attenuation ones with increasing x-ray energy), and a detailed dose optimization study should be conducted before the method can be applied clinically. However, we find that these preliminary results give an encouraging indication in terms of clinical compatibility.

Although we can obtain phase-retrieved images through two acquisitions,[25] we argue that a single, "mixed" image (like figure 2(b)) is sufficient to enable improved detection of breast abnormalities. This is the same strategy adopted by the aforementioned *in vivo* study with synchrotron radiation, [5] and has the advantage that radiologists can interpret the images by using the absorption signal as a reference.

In conclusion, we show that significant advances in mammography can be obtained at acceptable doses and exposure times, with moderate engineering development, using technology that is already commercially available.

Acknowledgments

This work is funded by the EPSRC (Grants EP/G004250/1 and EP/I021884/1) and by the Wellcome Trust (Grant 085856/Z/08/Z).

Conflict of interest

The authors declare no conflict of interest

References

[1]T. J. Davis, D. Gao, T. E. Gureyev, A. W. Stevenson, and S. W. Wilkins, "Phase-contrast imaging of weakly absorbing materials using hard x-rays," Nature **373**, 595-598 (1995).

[2]A. Snigirev, I. Snigireva, V. Kohn, S. Kuznetsov, and I. Schelokov, "On the possibilities of x-ray phase contrast microimaging by coherent high-energy synchrotron radiation," Rev. Sci. Instrum. **66**, 5486-5492 (1995).

[3]R. Lewis, "Medical phase contrast x-ray imaging: current status and future prospects," Phys. Med. Biol. **49**, 3573-3583 (2004).

[4]F. Arfelli, V. Bonvicini, A. Bravin, G. Cantatore, E. Castelli, L. Dalla Palma, M. Di Michiel, M. Fabrizioli, R. Longo, R. H. Menk, A. Olivo, S. Pani, D. Pontoni, P. Poropat, M. Prest, A.

Rashevsky, M. Ratti, L. Rigon, G. Tromba, A. Vacchi, E. Vallazza, and F. Zanconati, "Mammography with synchrotron radiation: phase detection techniques," Radiology **215**, 286-293 (2000).

[5]E. Castelli, M. Tonutti, F. Arfelli, R. Longo, E. Quaia, L. Rigon, D. Sanabor, F. Zanconati, D. Dreossi, A. Abrami, E. Quai, P. Bregant, K. Casarin, V. Chenda, R. H. Menk, T. Rokvic, A. Vascotto, G. Tromba, and M. A. Cova, "Mammography with synchrotron radiation: first clinical experience with phase-detection technique," Radiology **259**, 684-694 (2011).

[6]S. W. Wilkins, T. E. Gureyev, D. Gao, A. Pogany, and A. W. Stevenson, "Phase-contrast imaging using polychromatic hard x-rays," Nature **384**, 335-338 (1996).

[7]A. Olivo, F. Arfelli, G. Cantatore, R. Longo, R. H. Menk, S. Pani, M. Prest, P. Poropat, L. Rigon, G. Tromba, E. Vallazza, and E. Castelli, "An innovative digital imaging set-up allowing a low-dose approach to phase contrast applications in the medical field," Med. Phys. **28**,1610-1619 (2001).

[8]A. Olivo and R. Speller, "Experimental validation of a simple model capable of predicting the phase contrast imaging capabilities of an x-ray imaging system," Phys. Med. Biol. **51**, 3015-3030 (2006).

[9]T. Morita, M. Yamada, A. Kano, S. Nagatsuka, C. Honda, and T. Endo, "A Comparison Between Film-Screen Mammography and Full-Field Digital Mammography Utilizing Phase Contrast Technology in Breast Cancer Screening Programs," in *Lecture Notes in Computer Science*, edited by E. A. Krupinski (Springer, Berlin, 2008), pp. 48-54.

[10]D. Chapman, W. Thomlinson, R. E. Johnston, D. Washburn, E. Pisano, N. Gmür, Z. Zhong, R. Menk, F. Arfelli, and D. Sayers, "Diffraction enhanced x-ray imaging," Phys. Med. Biol. **42**, 2015-2025 (1997).

[11]C. Parham, Z. Zhong, D. M. Connor, L. D. Chapman, and E. D. Pisano, "Design and implementation of a compact low-dose diffraction enhanced medical imaging system," Acad. Radiol. **16**, 911-917 (2009).

[12]C. David, B. Nohammer, H. H. Solak, and E. Ziegler, "Differential x-ray phase contrast imaging using a shearing interferometer," Appl. Phys. Lett. **81**, 3287-3289 (2002).

[13]A. Momose, S. Kawamoto, I. Koyama, Y. Hamaishi, K. Takai, and Y. Suzuki "Demonstration of x-ray Talbot interferometry," Jpn. J. Appl. Phys. **42**, L866-L868 (2003).

[14]H. F. Talbot Facts relating to optical science. Philos. Mag. **9**, 401-407 (1836).

[15]F. Pfeiffer, T. Weitkamp, O. Bunk, and C. David, "Phase retrieval and differential phase-contrast imaging with low-brilliance x-ray sources," Nat. Phys. **2**, 258-261 (2006).

[16]M. Stampanoni, Z. Wang, T. Thüring, C. David, E. Roessl, M. Trippel, R. A. Kubik-Huch, G. Singer, M. K. Hohl, and N. Hauser, "The first analysis and clinical evaluation of native breast tissue using differential phase contrast mammography," Invest. Radiol. **46**, 801-806 (2011).

[17]J. Zambelli, N. Bevins, Z. Qi, and G.-H. Chen, "Radiation dose efficiency comparison between differential phase contrast CT and conventional absorption CT," Med. Phys. **37**, 2473-2479 (2010).

[18]A. Olivo and R. Speller, "A coded-aperture approach allowing x-ray phase contrast imaging with conventional sources," Appl. Phys. Lett. **91**, 074106 (2007).

[19]K. Ignatyev, A. Olivo, P. R. T. Munro, and R. D. Speller, "X-Ray Imaging: method for highly accurate automated geometric alignment of masks and detector," International Patent WO/2013/011316, Jan 24 2013.

[20]A. Olivo, K. Ignatyev, P. R. T. Munro, and R. D. Speller, "Noninterferometric phase-contrast images obtained with incoherent x-ray sources," Appl. Opt. **50**, 1765-1769 (2011).

[21]A. Olivo and R. Speller, "Modelling of a novel x-ray phase contrast imaging technique

based on coded apertures," Phys. Med. Biol. **52**, 6555-6573 (2007).

[22]R. J. Dejus and M. Sanchez del Rio, "XOP: A graphical user interface for spectral calculations and X-ray optics utilities," Rev. Sci. Instrum. **67**, 3356 (1996).

[23]J. Boone, "Glandular breast dose for monoenergetic and high-energy x-ray beams: Monte Carlo assessment," Radiology **213**, 23-37 (1999).

[24]G. Gennaro, P. Baldelli, A. Taibi, C. Di Maggio and M. Gambaccini, "Patient dose in full-field digital mammography: an Italian survey," Eur. Radiol. **14**, 645-652 (2004).

[25]P. R. T. Munro, K. Ignatyev, R. D. Speller, and A. Olivo, "Phase and absorption retrieval using incoherent x-ray sources," Proc. Natl. Acad. Sci. **109**, 13922-13927 (2012).